Low-frequency dynamical heterogeneity in simulated amorphous $Ni_{0.5}Zr_{0.5}$ below its glass temperature: Correlations with cage volume and local order fluctuations

I. Ladadwa* and H. Teichler†
Institut für Materialphysik and SFB 602, Universität Göttingen, 37077 Göttingen, Germany
(Received 11 October 2005; published 2 March 2006)

From molecular dynamics simulations results are reported concerning correlations between low-frequency (*lf*) heterogeneous dynamics in simulated $Ni_{0.5}Zr_{0.5}$ melts at 700, 760, and 810 K, which means around the Kauzmann temperature of the model, $T_K \approx 750$ K. A method is presented to separate *lf* dynamics, reflecting the slow relaxation dynamics in the vitrifying melt, and high-frequency (*hf*) dynamics, characteristic of the thermal fluctuations at the considered temperatures. By means of a suitable quantitative measure of the distribution of heterogeneous *lf* dynamics in space and time, correlation parameters are evaluated between the spatial distribution of *lf* dynamics and structural inhomogeneities in the thermodynamically homogeneous melt. Relevant correlations are found between *lf* dynamics and some involved structure quantities such as the cage volume around Ni atoms, Ω_{Ni}, or the Θ_{Ni} parameter which reflects the geometry of the nearest-neighbor cage around Ni atoms. Further, at 810 K there is a weak correlation between heterogeneous dynamics and fluctuations of the mean potential energy per atom and a comparable weak anticorrelation with the particle density and Ni-atom density inhomogeneities, where these three correlations decrease with decreasing temperature. The present results indicate the existence of long-living regions of enhanced Ω_{Ni} in the structure, which may act as regions of preferential initiation of irreversible *lf* dynamics and slow relaxation.

DOI: 10.1103/PhysRevE.73.031501 PACS number(s): 64.70.Pf, 61.20.Ja, 61.20.Lc

I. INTRODUCTION

In the context of the glass transition, dynamical heterogeneity has been proposed by Adam and Gibbs [1] as the fundamental phenomenon characterizing the processes that lead to the dramatic slowing down of structural dynamics inherent to vitrification. Despite the enormous importance to understand these processes for understanding the glass transition and while there exist a number of experimental studies (e.g., [2–4]) and some molecular dynamics (MD) simulations (e.g., [5–9]) about dynamical heterogeneity in undercooled melts, a conclusive answer has been missing so far concerning the relationship between the dynamical heterogeneity and local structure properties of the system. Regarding this, in a recent paper [10], Ediger [2] is cited with the statement "At present it is an article of faith that something in the structure is responsible for dynamics that can vary by orders of magnitude from one region of the sample to another at T_g." Here, some clarification has been achieved by Widmer-Cooper, Harrowell, and Fynewever [10] from their MD analysis of a two-dimensional soft-sphere model, where they provide obvious evidence for an interdependence between a given configuration of particles and their subsequent dynamics. But there remains the problem to uncover the link between the tendency of atoms to become mobile or remain immobile and specific structural features of the configuration. There is the additional complication that one has to filter out from all fluctuations the low-frequency processes carrying the slow dynamics of the system and to analyze their relationship to inhomogeneities in the structure.

In the literature, there exist only a few studies concerning the relationship between dynamical heterogeneity and structural properties in the liquids. Although leaving the answer open, recently Ediger [2] discussed the point in rather general terms and distinguished two categories of possible sources: density and configuration-entropy fluctuations on the one hand and on the other hand frustration-limited domain and energy landscape phenomena. Beyond mere classification, more specific information has been obtained from experimental studies of the glass transition for colloidal systems. Weeks and Weitz [3] confirmed that rearrangements of the cages around given particles involve the cooperative motion of groups of neighboring species, where mobile atoms tend to be in regions of higher disorder, lower density, and higher free volume. In contrast to this, Sood [4] reports earlier studies concerning structural ordering in colloidal suspensions which indicate for a hard-sphere-like system that the free volume around particles in ordered regions is greater than in disordered ones.

Important additional information in this field has been gained from recent MD studies. From investigating the relation of local energy and composition versus mobility, Donati *et al.* [5] deduced that the mobility of atoms increases when their potential energy increases. While this observation confirms the existence of a link between mobility and local atomic environment, Perera and Harrowell [6], from investigating local structures and local relaxation times in computer-simulated two-dimensional glass-forming mixtures, come to the conclusion that there is no correlation between these two quantities at high temperatures and only some weak correlation at low temperatures for the larger, less-mobile particles. Vollmayr-Lee, Kob, and Zippelius [7] approached the question of what inhibits a particle to become mobile by analyzing the coordination number of mobile and immobile particles and come to the conclusion that mobile particles have the tendency, on average, to be caged by fewer neighbors than an average particle of the same kind will be.

*Electronic address: imad@ump.gwdg.de
†Electronic address: teichler@ump.gwdg.de

The analysis [8] of the spatial distribution of vibration modes in amorphous argon indicates that the low-frequency shoulder increases in the partial spectrum of the imperfect part of structure. This reflects that the low-frequency modes have large amplitudes at atoms with imperfect surroundings and that they are less intense at atoms with perfect surroundings, which may be used as an indication for weaker cages around the particles in imperfect surroundings. Additional important information was obtained by Büchner and Heuer [9] from studying the correlation between the topography of the potential energy landscape of supercooled liquids and their dynamics in space. The analysis revealed that in the supercooled regime the dynamics is strongly affected by the presence of deep valleys in the energy landscape, leading to long-living metastable amorphous states.

The present contribution reports some of our recent MD results in this field, which concern, in particular, correlations between the heterogeneity of dynamics in a simulated, vitrifying $Ni_{0.5}Zr_{0.5}$ system and microscopic quantities of the underlying atomic structure like cage size around the atoms, local order fluctuations, or local particle densities. There is a significant difference between the MD simulations mentioned above and our present approach. The former consider liquids at temperatures in the range of the critical temperature T_c of mode-coupling theory [11] or liquid configurations deduced by simulated ultrarapid quenching from such temperatures. We analyze well-relaxed samples aged at 810, 760, and 700 K, markedly below T_c, which for the present model is found at 1120 K [12,13], in a temperature range reaching down to Kauzmann's [14] temperature T_K, estimated to be around 750 K [15] for the model. While the former samples have α-decay relaxation times in the nanosecond range, our samples show τ_α values in the microsecond regime [16]. According to that, like in our recent study [16], the present samples are characterized by extreme slow irreversible structural dynamics which take place on a time scale separated by more than three orders of magnitude from the time scale of thermally activated reversible structural fluctuations. That means we here analyze heterogeneous dynamics in an advanced state of glass formation, approaching the pseudosolid regime, while the analysis around T_c considers a significantly earlier state.

The article is organized as follows: in Sec. II a brief description of the methods and model shall be given, providing a description of how mobility of particles is characterized and how dynamical heterogeneity is measured. We also briefly illustrate the microscopic parameters used to characterize quantitatively the underlying atomic arrangement. Section III presents the results of the MD analysis, including cross-correlation values among the various quantities. Section IV is devoted to a discussion of the results, and Sec. V gives some concluding remarks.

II. MODEL AND METHODS OF DATA ANALYSIS

The MD calculations are carried out as isothermal-isobaric (N,T,p) simulations for a binary $Ni_{0.5}Zr_{0.5}$ alloy with zero pressure. The equations of motion are integrated numerically by a fifth-order predictor-corrector algorithm with time step $\Delta t = 2.0 \times 10^{-15}$ s. An ensemble of $N=5184$ atoms is considered in an orthorhombic box with periodic boundary conditions and box lengths evaluated from a zero-pressure condition. Three systems with different temperatures 700, 760, and 810 K have been simulated over a time range up to 1.0 μs. The simulations were performed using pair potentials adapted to Hausleitner-Hafner potentials [17]. The starting structure at 810 K is taken from [18] and was prepared as described there. The structure at 760 K is obtained from the 810 K sample by isothermal annealing for 0.6 μs and subsequent quench with 10^{10} K/s to 760 K.The sample at 700 K is generated by isothermal annealing the 760-K structure for 0.6 μs followed by a quench to 700 K with 10^9 K/s. Further details about the method may be found in Refs. [12,13,15,19,20]

A. Mobility

Our definition of atomic mobility takes advantage of the fact that we are interested primarily in the slow, low-frequency atom motions relevant for the irreversible structure changes in the melt. Therefore, as in [16], all kinds of vibrations and reversible high-frequency motions are eliminated by averaging over the trajectories of the atoms and introducing smoothed atomic paths $\vec{\bar{r}}_n(t)$ by the low-pass filter:

$$\vec{\bar{r}}_n(t) = \int_{-\infty}^{\infty} \vec{r}_n(t') \frac{e^{(t-t')^2/2\tau^2}}{\sqrt{(2\pi\tau^2)}} dt' . \tag{1}$$

From the $\bar{r}_n(t)$, a suitable measure of the momentary mobility of a particle can be introduced as

$$\delta w_n(t)^2 = \int_{-\infty}^{\infty} [\vec{\bar{r}}_n(t) - \vec{\bar{r}}_n(t')]^2 \frac{e^{(t-t')^2/2\tau^2}}{\sqrt{(2\pi\tau^2)}} dt' , \tag{2}$$

where for the present purposes $\tau=3$ ns turned out as an appropriate choice.

This definition of mobility, used throughout in our study, allows us to characterize all atoms and to ascribe to each of them a quantitative value of mobility as a continuous function of time. Figure 1 demonstrates the effects of Eqs. (1) and (2): The plot shows the trajectories $x_n(t)$ and $\bar{x}_n(t)$ of a particular atom; while the original trajectory involves all vibrations and fluctuations, the low-pass-filtered smoothed one presents the long-time dynamics only. The averaged positions are then used to calculate the mobility as stated in Eq. (2). Figure 1 demonstrates the occurrence of large values $\delta w_n(t)^2$ at times t around which large changes in $\bar{r}_n(t)$ take place.

In addition to the mobility per particles, $\delta w_n^2(t)$, we introduce in r space the density

$$\delta w^2(\vec{r},t) = \sum_n \delta w_n^2(t)\, \delta(\vec{r} - \vec{r}_n(t)) \tag{3}$$

and analogously the particle density

$$\delta\rho(\vec{r},t) = \sum_n \delta(\vec{r} - \vec{r}_n(t)) . \tag{4}$$

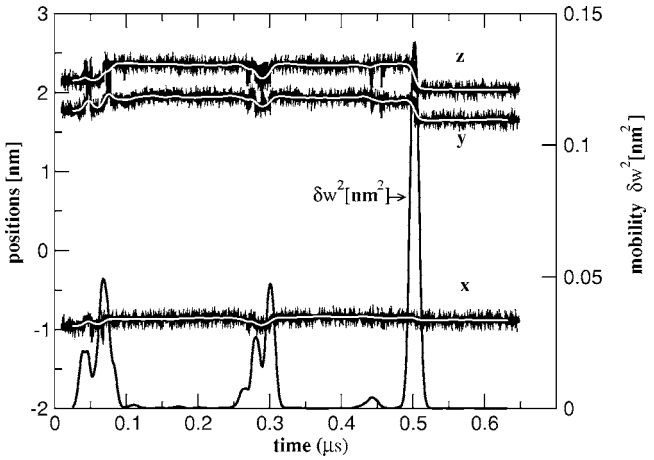

FIG. 1. Steps of mobility definition: Noisy black lines: original $x_n(t)$, $y_n(t)$, and $z_n(t)$ positions of particle n. White lines: smoothed positions $\bar{x}_n(t)$, $\bar{y}_n(t)$, and $\bar{z}_n(t)$ of the same particle. Solid line: mobility $\delta w_n(t)^2$ (left-hand scale, positions; right-hand scale, mobility strength).

From these quantities we deduce an averaged mobility of the atoms during the time interval $[t_1,t_2]$:

$$\delta w^2(\vec{r},t_1,t_2) = \frac{\int_{t_1}^{t_2} \delta w^2(\vec{r},t)dt}{\int_{t_1}^{t_2} \delta\rho(\vec{r},t)dt}, \tag{5}$$

where in the numerical evaluation a coarse-graining scheme is used by dividing the simulation box into 27 000 small cells, 30 in each direction. For a suitable selected time interval $[t_1,t_2]$ a mobility value is ascribed to each cell by summing over the mobility of all atoms that cross this cell during $[t_1,t_2]$. In the next step this mobility value is normalized by the averaged number of particles in the cell during $[t_1,t_2]$ to get the mean mobility value per particle. The same technique is used to calculate the spatial distribution of further quantities, like the local order fluctuations and the local atomic volume described in Secs. II C and II B, respectively. This kind of partitioning of the simulations box into small cells of equal size is used for constructing three-dimensional space contour plots for the parameters and for estimating the correlation coefficients described in Sec. II D.

B. Atomic volume distribution

As a particular tool to characterize the structural inhomogeneity in the thermodynamically homogeneous liquid phase, we use the atomic volume per atom, $\Omega_n(t)$. For $\Omega_n(t)$ two different measures are adopted, either the volume of the Voronoi cell [21] at time t around atom n, $\Omega_n^V(t)$, or Egami's estimate $\Omega_n^E(t)$ [22,23] defined by

$$\Omega_n^E(t) = (4\pi/3)\left(\frac{\sum_{j\in NN} r_{nj}^{-1}}{2\sum_{j\in NN} r_{nj}^{-2}}\right)^3. \tag{6}$$

The summation runs over the atoms in the nearest-neighbor shell and r_{nj} means the interatomic distances in smoothed coordinates. When evaluating Eq. (6) we treat as nearest neighbors all atoms with smoothed distance $|\vec{r}_n-\vec{r}_m|$ less than the first minimum in the radial distribution function. From $\Omega_n^V(t)$ and $\Omega_n^E(t)$ we obtain the averaged volume distribution function $\Omega_{Ni}^{V/E}(\vec{r},t_1,t_2)$ at $\vec{r}$ during the time interval $[t_1,t_2]$ by following Eqs. (3)–(5). We introduce, in particular, the distribution of the atom volume around Ni atoms:

$$\Omega_{Ni}^{V/E}(\vec{r},t_1,t_2) = \frac{\int_{t1}^{t2} \Omega_{Ni}^{V/E}(\vec{r},t)dt}{\int_{t1}^{t2} \rho_{Ni}(\vec{r},t)dt}, \tag{7}$$

$$\Omega_{Ni}^{V/E}(\vec{r},t) = \sum_{n'} \Omega_{n'}^{V/E}(t)\,\delta(\vec{r}-\vec{r}_{n'}(t)), \quad n' \in Ni, \tag{8}$$

and $\rho_{Ni}(r,t)$ from Eq. (4) by restricting the summation over Ni atoms, only.

C. Local structure order distribution

As proposed by Steinhardt *et al.* [24], a characterization of the local structure in an amorphous system can be given by the order parameters

$$Q_l(n,t) = \left[\frac{4\pi}{2l+1}\sum_{m=-l}^{l} |\langle Y_{lm}(\theta_{nk},\phi_{nk})\rangle|^2\right]^{1/2}. \tag{9}$$

$Y_{lm}(\theta_{nk},\phi_{nk})$ are spherical harmonics. k labels the atoms in the nearest-neighbor shell of n. θ_{nk}, ϕ_{nk} indicates the direction from n to the kth neighbor in an arbitrary, fixed frame. The brackets $\langle\cdot\rangle$ mean averaging over k.

In our analysis we take care of the fact that in the Zr-rich and in the middle-concentration amorphous $Ni_{0.5}Zr_{0.5}$ melts, the Ni atoms reside with large probability in trigonal prismatic environments, as in the crystalline $Ni_{0.5}Zr_{0.5}$ equilibrium structure with $B33$ symmetry.

In order to analyze the probability of local trigonal structure, we introduce in addition to Q_4 and Q_6 the combined parameter

$$\Theta(n,t) = \exp\{-[Q_6(n,t)/Q_6^{tp}-1]^2 - [Q_4(n,t)/Q_4^{tp}-1]^2\}, \tag{10}$$

where $Q_6^{tp}=0.4742$ and $Q_4^{tp}=0.3990$ are the corresponding parameter values for a nearest-neighbor shell in a perfect trigonal-prismatic arrangement. From this definition of $\Theta(n,t)$ we deduce an averaged value $\Theta_{Ni}(\vec{r},t_1,t_2)$ for the Ni atoms in $\vec{r}$ during the interval $[t_1,t_2]$, by using similar steps as in Eqs. (3)–(5),

$$\Theta_{Ni}(\vec{r},t_1,t_2) = \frac{\int_{t1}^{t2} \Theta_{Ni}(\vec{r},t)dt}{\int_{t1}^{t2} \rho_{Ni}(\vec{r},t)dt}. \tag{11}$$

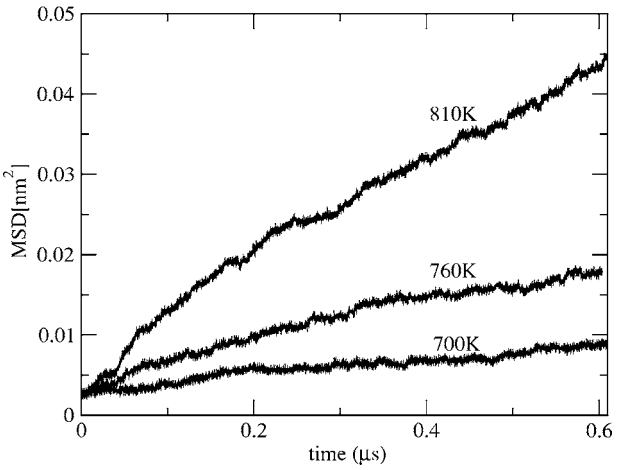

FIG. 2. Mean-square displacement for Ni atoms in simulated $Ni_{0.5}Zr_{0.5}$ at temperatures $T=810$, 760, and 700 K.

D. Correlations

Correlations between the local heterogeneous mobility and further spatial distributions are evaluated by

$$R(X,Y) = \frac{\langle XY\rangle - \langle X\rangle\langle Y\rangle}{[\sqrt{\langle X^2\rangle - \langle X\rangle^2}][\sqrt{\langle Y^2\rangle - \langle Y\rangle^2}]}. \tag{12}$$

Here the brackets $\langle\cdot\rangle$ stand for averaging over r, which means over the volume of the simulation box V,

$$\langle XY\rangle = V^{-1}\int d^3\vec{r}X(\vec{r})Y(\vec{r}). \tag{13}$$

X and Y stand for the quantities $\delta w(\vec{r},t_1,t_2)^2$, $\Omega_{Ni}(\vec{r},t_1,t_2)$, and $\Theta_{Ni}(\vec{r},t_1,t_2)$ taken from the same or from different time intervals $[t_1,t_2]$.

III. RESULTS

A. Mean-square displacement

Figure 2 displays the mean-square displacement (MSD) for Ni atoms in the present system with $N=5184$ atoms in the simulation box. Presented are the data in a time interval of $0<t<0.6$ μs at 700, 760, and 810 K. Use of the relation [25]

$$D_{Ni}(T) = \frac{1}{6}\lim_{t\to\infty}\partial_t\langle u^2(t)\rangle \tag{14}$$

yields for the diffusion coefficients $D_{Ni}(T)$ a value of 1.1×10^{-15} m^2/s at 700 K (6×10^{-15} and 1.1×10^{-14} m^2/s at 760 and 810 K), where the slope is taken from the approximately linear regime $0.2<t<0.6$ μs.

The present data for $D_{Ni}(T)$ fit rather well to the estimates of the $D_{Ni}(T)$ in [19]. This indicates that the Ni dynamics found in the present system is of realistic order of magnitude compared to the extrapolation from experimental data [26], as are the data in [19]. The intermittent dynamics characteristic for the $N=648$ atoms system in [16,19] is no longer visible in the MSD of 5184 atoms in Fig. 2. Apparently, this particle number is sufficiently large to average out the intermittency. In order to test this, we have divided the total system of 5184 atoms into 8 different octants with 648 atoms on average. Figure 3 presents the eight MSD curves obtained for these octants. They indeed show intermittent dynamics. There is, in particular, a striking similarity between the MSD curve of octant D and the data in [19] for 700 K. The mutual geometric interrelationship between the eight octants $A,\ldots,H$ is given by Fig. 5(a), below, where the corresponding labels are attached to the simulation box edges.

B. Heterogeneous mobility

A representative plot of the heterogeneous mobility in the simulated vitrifying $Ni_{0.5}Zr_{0.5}$ model at 810 K is shown in Fig. 4(a) for the time interval $J_0=[0,0.6\ \mu s]$. Figure 4(a) displays the distribution of mobile atoms in the simulation box. An atom is named "mobile" in the considered time interval if its mobility parameters $\delta w_n^2(t)$ exceeds a critical value in the interval, which means if

$$\delta w_n^2(t)\big|_{t_1<t<t_2} \geqslant \delta w_c^2(t_1,t_2). \tag{15}$$

The value of δw_c^2 is fixed by demanding that the number of mobile atoms in the considered time interval equal 5% of the total number of atoms. Regarding the definition of mobile atoms we at this point follow the approach used in, e.g., Refs. [5,7,27], as it is the purpose of Fig. 4 to indicate that our treatment identifies as a region of enhanced mobility just the regions with an enhanced density of mobile atoms according to the definition of, e.g., Refs. [5,7,27]. At the considered temperature of 810 K, only Ni atoms fulfill the criterion for being mobile. Figure 4 indicates that most of the mobile atoms group together and form local clusters with a typical diameter of about 1–2 nm. Figure 4(b) gives for the same time interval a contour plot of $\delta w^2(\vec{r},t_1,t_2)$ according to Eq. (5). The contour lines correspond to $\delta w^2(\vec{r},t_1,t_2)/\langle\delta w^2(\vec{r},t_1,t_2)\rangle=13.0$, 11.0, 7.0, 2.5, where $\langle\delta w^2(\vec{r},t_1,t_2)\rangle$ means the average over all $\vec{r}$. The cores represent the highest value; the mobility decreases with distance from the core. Figure 4(b) gives direct evidence for dynamical heterogeneity.

There is a large similarity between the distribution of mobile atoms in Fig. 4(a) and the regions of large mobility $\delta w^2(\vec{r},t_1,t_2)$ in Fig. 4(b). In particular, one finds an accumulation of mobility in those volume regions where the mobile atoms have grouped together and form clusters.

Figures 5(a)–5(c) presents the heterogeneous mobility $\delta w^2(\vec{r},t_1,t_2)$ at 700 K for three different time intervals of evolution of the system: Figure 5(a) shows $t\in I_1=[0.3,0.45\ \mu s]$, Fig. 5(b) displays $t\in I_2=[0.45,0.6\ \mu s]$, and Fig. 5(c) gives $t\in I_0=[0,1.0\ \mu s]$. The displayed contour lines correspond to $\delta w^2(\vec{r},t_1,t_2)/\langle\delta w^2(\vec{r},t_1,t_2)\rangle$ as in Fig. 4(b). All drawings in Fig. 5 show the identical projection of the simulation box. In Fig. 5(a) the labels $A,\ldots,H$ at the simulation box edges correspond to the labels used in Fig. 3 for the eight octants of the box.

From a comparison of Figs. 5(a) and 5(b) it is obvious that the heterogeneous mobility has changed between time interval I_1 and interval I_2. Regions of enhanced mobility in I_1

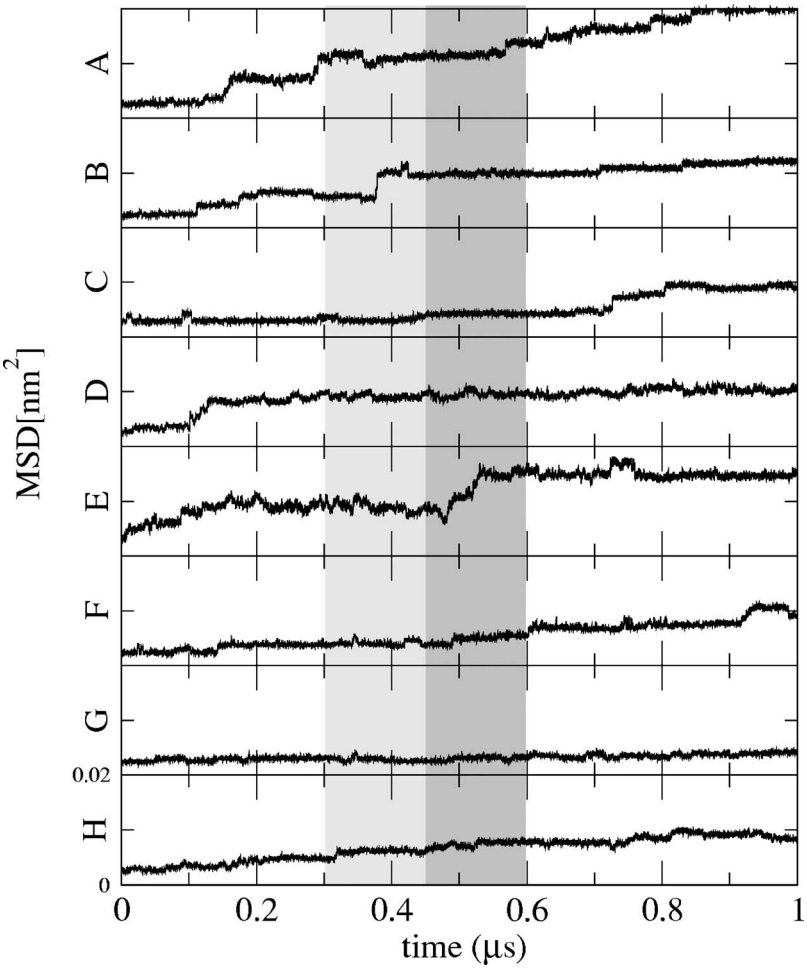

FIG. 3. Simulated MSD curves for Ni in amorphous $Ni_{0.5}Zr_{0.5}$ at 700 K obtained for the eight octants with 648 atoms on average in the $N=5184$ system. The curves show marked intermittent dynamics $A,\ldots,H$ label the eight octants indicated in [Fig. 5(a)].

are at rest in I_2 and vice versa, where there is also visible a mobile region which is displaced in space from I_1 to I_2. According to Fig. 5(a), the heterogeneous dynamics in the time interval I_1 mainly is due to a dynamical event in octant B with fringes in A and D and an event in octant E with fringes in G. The dynamics in the later time interval I_2 are caused by an event in octant E with fringes in F and A. These conclusions from Figs. 5(a) and 5(b) agree well with the MSD in the octants given in Fig. 3. In Fig. 3 the intervals I_1 and I_2 are indicated by light grey stripes. According to Fig. 3 there obviously are dynamical events in I_1 in the octants A, B, and E while in I_2 the main activity takes place in octant E with contributions in A, F, and H.

C. Cage size around Ni atoms

As described in Sec. II B, the spatial distribution of the cage size volume around the Ni atoms is used as one tool to characterized fluctuations in the structure of the thermodynamically homogeneous melt. Figures 5(d)–5(f) present contour lines of the Egami cage volume size around Ni atoms at 700 K for the three time intervals I_1, I_2, and I_0. The provided four contour lines correspond to the normalized values $\Omega^E_{Ni}(r,t_1,t_2)/\langle\Omega^E_{Ni}(r,t_1,t_2)\rangle=1.55$, 1.4, 1.3, and 1.2, respectively, where the brackets mean averaging over the simulation box. Comparison of Figs. 5(a) and 5(d), 5(b) and 5(e), and 5(c) and 5(f) makes obvious a striking similarity between mobility distribution and cage-size distribution in each of the intervals I_1, I_2, and I_0. In particular, the change of the mobility distribution between I_1 and I_2, which means the time evolution of the mobility distribution, is reflected by the change of the cage-size distribution $\Omega^E_{Ni}(r,t_1,t_2)$ from I_1 and I_2.

D. Local structure around Ni atoms

The local structure around Ni atoms is characterized, in addition, in terms of the order parameters Q_6, Q_4, and the Θ_{Ni} parameter deduced there from according to Eq. (9). Figure 6(a) shows a plot of probability of Q_4 and Q_6 values at Ni atoms from our modeling at $T=700$ K in the time interval I_1, which takes into account all Ni atoms. Figure 6(b) provides the corresponding distribution for the highly mobile Ni atoms in this interval, where highly mobile means those atoms that belong to the 5% with the highest mobility in this time window. For the highly mobile atoms there is a shift in Q_6 towards higher values and a second peak and wing at higher values of the Q_4 distribution. For the combined parameter Θ_{Ni}, Eq. (10), the difference in the Q_4 and Q_6 distribution of highly mobile and of averaged Ni atoms yields a marked difference in the probability distribution of Θ_{Ni} values, $P(\Theta_{Ni})$, for highly mobile and average Ni atoms. Figure

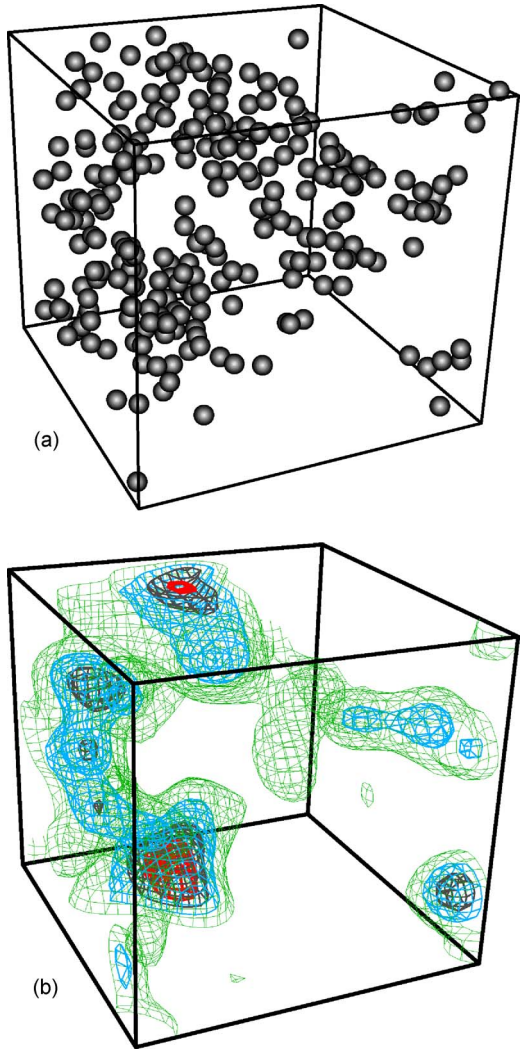

FIG. 4. (Color online) (a) Distribution of mobile atoms at $T=810$ K (mobile atoms here mean the upper 5% of atoms with largest mobility, in accordance with Refs. [5,7,27]). (b) 3D contour plot for total mobility at $T=810$ K. The two figures show the same projection in order to demonstrate the resemblance between the contour and distribution of the mobile atoms.

7 displays the corresponding distributions. The figure indicates that for the highly mobile atoms $P(\Theta_{Ni})$ is shifted towards higher Θ_{Ni} values. According to this, a spatial region of highly mobile atoms should be visible as regions of increased mean Θ_{Ni} value. Figures 5(g)–5(i) display contour lines of the distribution of Θ_{Ni} values in space at 700 K for the time intervals I_1, I_2, and I_0. The spatial distribution of Θ_{Ni} values looks rather similar to the distribution of Ω_{Ni}^E values shown in Figs. 5(d)–5(f), and there is a close similarity in the distribution of Θ_{Ni} values and the mobility distribution in space. Like the distribution of Ω_{Ni}^E values, the distribution of Θ_{Ni} values changes with time when going, e.g., from I_1 to I_2, where the changes are parallel to the changes in the mobility.

E. Correlation values

In order to describe quantitatively the similarity between the spatial distribution of atomic mobility δw^2, Ω_{Ni}^E values, and Θ_{Ni} parameter, we use the correlation parameters of Eq. (12). As indicated in Sec. II A, these quantities are evaluated on a coarse-grained three-dimensional (3D) grid with 27 000 nodes in the simulation box. Table I presents the correlation parameters from our 700-K MD simulations for the three time intervals I_0, I_1, and I_2 of Fig. 5 determined by substituting the spatial integration with summation over the coarse-graining grid. For all three intervals there is a strong correlation between the spatial fluctuations in the Ω_{Ni}^E, Θ_{Ni}, and Voronoi-cell Ω_{Ni}^V distributions. Correlation values R between Ω_{Ni}^E and Θ_{Ni}, not shown in Table I, turn out around 0.95, values between Ω_{Ni}^E and Ω_{Ni}^V around 0.9. These correlations indicate that these parameters reflect similar aspects of the structure. The spatial inhomogeneity of these quantities is markedly correlated with the heterogeneity of the mobility in all considered time intervals, with correlation parameter values between 0.53 and 0.77.

Table I also includes cross-correlation parameters between the atomic mobility δw^2 and the inhomogeneities in the total particle density ρ_{par} and the Ni-atom density ρ_{Ni}. Here R values are close to zero, which indicates that at this temperature in the low-frequency range no reliable correlations exist between these structural parameters and particle mobility. Further entries in Table I concern autocorrelations of Θ_{Ni} and δw^2 between the different time intervals I_1 and I_2 which means changes of the spatial fluctuations with time. The related R values are 0.5 for Θ_{Ni} and 0.15 for δw^2. They indicate a moderate decay of spatial inhomogeneities with time in the Θ_{Ni} distribution and a strong decay with time in the heterogeneous dynamics.

For estimating the order of magnitude of variations with time in the correlations between dynamical and structural heterogeneity, we have evaluated in addition the cross-correlation value $R(\delta w^2, \Omega_{Ni}^V)$ for a third independent time interval $I_3: t \in [0.6, 0.75\ \mu\text{s}]$, finding $R \approx 0.51$. Together with the data for I_1 and I_2 from Table I, this value leads to the mean of 0.57 with standard deviation ± 0.05 for the cross correlations between structural and dynamical heterogeneity at 700 K in time intervals of 0.15 μs length for the present degree of the aging. The larger R values in Table I for the time interval I_0 of 1 μs length may be taken as an indication of stronger correlations in space than in space-time.

Correlation parameters at different temperature are compiled in Table II, which compares the resulting values for 700, 760, and 810 K. Table II considers a longer time interval J_0 of 0.6 μs and two short intervals J_1 and J_2 of 0.1 μs each. The observations in Table II are in fair agreement with the data given in Table I for the intervals I_0–I_2. There is the general trend that the correlations tend to be larger at 810 K, giving evidence that at higher temperatures in the low-frequency range some anticorrelation exists between heterogeneous dynamics and the inhomogeneity in the spatial distribution of total particle density ρ_{par} and the Ni-atom density ρ_{Ni}. A similar result is found for the correlation between the heterogeneous distribution of mobility in space, δw^2, and the inhomogeneous distribution of the mean potential energy per atom, E_{pot}. Here the correlation value increases from 0.05 to 0.33 between 700 and 810 K, supporting the assumption that there may exist a marked correlation between these quantities at higher temperatures.

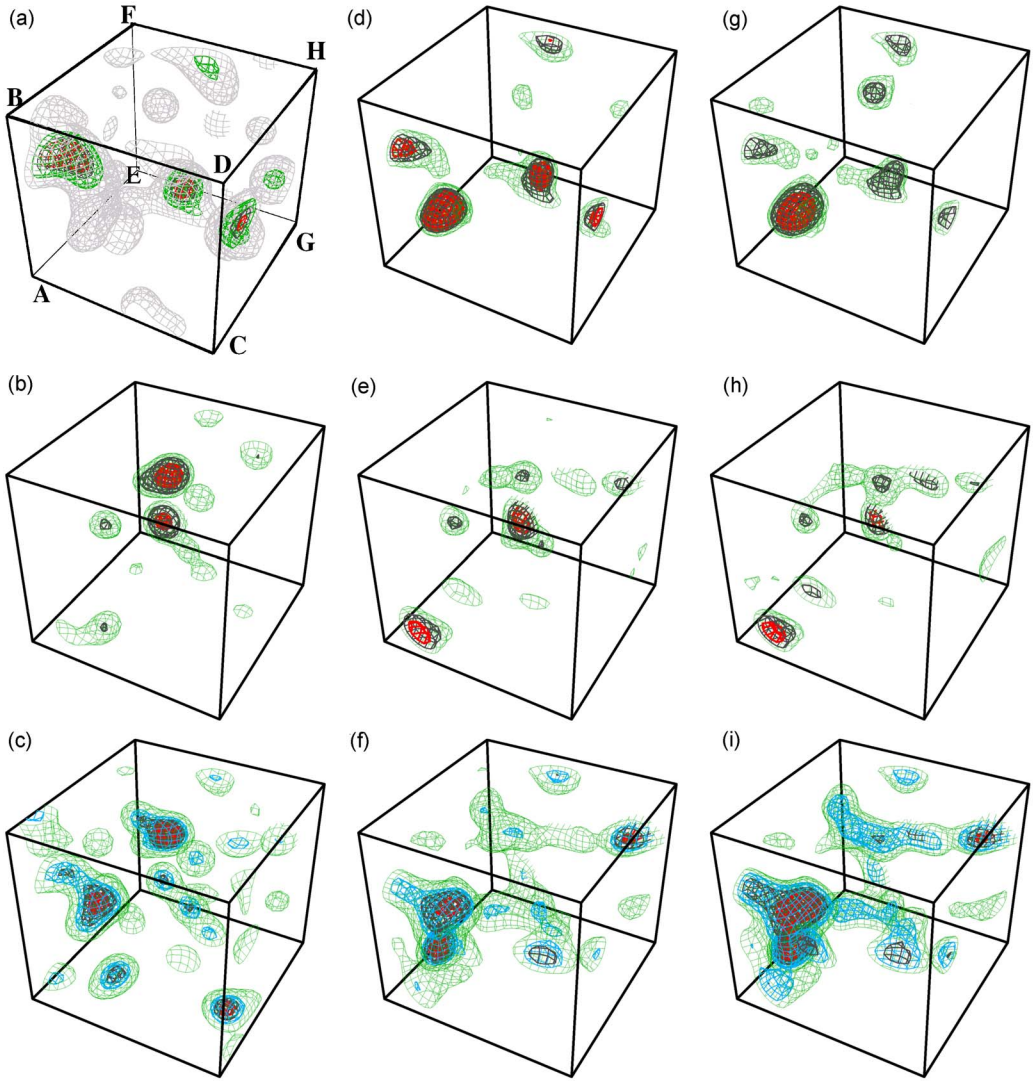

FIG. 5. (Color online) Heterogeneous distribution of mobility and structural inhomogeneities in simulated $Ni_{0.5}Zr_{0.5}$ at 700 K. (a) Distribution of mobility for time interval 0.3–0.45 μs. (b) Like (a) but for the simulated time interval 0.45–0.6 μs. (c) Mobility distribution for the total simulated time 0–1.0 μs. (d) Distribution of parameter Θ_{Ni} for time interval 0.3–0.45 μs. (e) Distribution of parameter Θ_{Ni} for time interval 0.45–0.6 μs. (f) Distribution of parameter Θ_{Ni} for the total simulated time. (g) Distribution of cage volume around Ni atoms for the time interval 0.3–0.45 μs. (h) Like (g) but for the time interval 0.45–0.6 μs. (i) Like (g) but for the total simulated time.

F. Change of correlations with time

In order to analyze more properly the change of correlations with time, we use correlation parameters $R(X(t_i,\Delta t),X(t_f,\Delta t))$, which measure the correlation of the spatial distribution of quantity X in time interval $[t_i,t_i+\Delta t]$ with its distribution in time interval $[t_f,t_f+\Delta t]$. Figure 8(a) presents the resulting data for the mobility distribution (indicated by squares) and the cage volume around Ni atoms (indicated by circles) at 700 K. In Fig. 8(a), t_i is fixed at 0.35 μs while t_f varies from 0.35 to 0.42 μs. The $R(X(t_i,\Delta t),X(t_f,\Delta t))$ are shown as a function of t_f. Two different lengths of the time interval are considered: $\Delta t_1 = 0.1$ μs (open squares and circles) and $\Delta t_2 = 0.07\mu$s (solid symbols). At $t_f = t_i = 0.35$ μs, the correlation value is normalized to one by definition. Figure 8(a) makes obvious that the correlation in the mobility distribution decays with time delay $t_f - t_i$ more rapidly and more strongly than the correlation in the cage volume distribution. This is an indication for a long-living component in the spatial inhomogeneity of the cage volume distribution, which either exists independently of the atomic mobility or reflects a long-living remainder of the latter.

More detailed information on the change of correlations can be gained from comparing the results from time interval Δt_1 with those from Δt_2. In case of the mobility, the R values in Fig. 8(a) from the intervals of different length Δt_α reflect a common decay in the correlations around $t_f \approx 0.375$ μs and a split decay around $t_f \approx 0.39$ μs and $t_f \approx 0.42$ μs. These observations can be interpreted as that around $t_f \approx 0.375$ μs the final interval $[t_f,t_f+\Delta t_\alpha]$ is shifted so much against t_i that it leaves a time region of particular mobility, independent of its length Δt_α. Hence this must be an event that takes place around 0.375 μs. The split decay around $t_f \approx 0.39$ μs and $t_f \approx 0.415$ μs can be interpreted as that the shifted intervals enter a time region of particular mobility located in time at

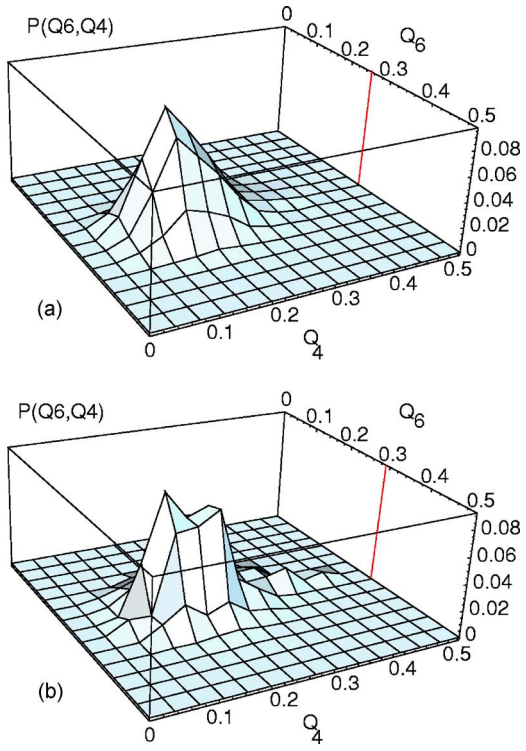

FIG. 6. (Color online) Probability of Q_4 and Q_6 values around Ni atoms in simulated $Ni_{0.5}Zr_{0.5}$ at 700 K (a) for all Ni atoms and (b) for Ni atoms of high mobility.

$t_f+\Delta t_\alpha$ which thus should be located around 0.49 μs. Indeed, from inspection of Fig. 3 we see that the mean-square displacements reflect an event with increased structural changes, which means local mobility, around 0.38 μs in octants A and B, and that there starts a large event of local mobility around 0.48 μs in octant E.

The slow and smooth decay of the correlation parameters R for the atom cage volume indicates, as already mentioned, a long-living component in the cage volume distribution. Apparently, the mobility event around 0.375 μs has no particular effect on the change of the cage-size distribution. On the other hand, for t_f above 0.405 μs, there is a difference in the correlation parameters for the two different Δt_α values. This may be taken as an indication that the longer interval now enters a time region of modified spatial distribution in the cage size, which means that the event starting around 0.48 μs in octant E might influence and change the distribution of the Ni cage volume.

More details about correlations in the time evolution of heterogeneous dynamics and structural inhomogeneity can be deduced by directly comparing $\delta w^2(\vec{r},t,t+\Delta t_2)$ and, e.g., $\Omega_{Ni}^E(\vec{r},t,t+\Delta t_2)$ in time and space. As described in Sec. II, the quantities $\delta w^2(\vec{r},t,t+\Delta t_2)$ and $\Omega_{Ni}^E(\vec{r},t,t+\Delta t_2)$ are available in space as coarse-grained data on a 3D grid with 27 000 nodes in the simulation box, which means in each direction 30 points with distance $\Delta L_\nu=L_\nu/30(\nu=x,y,z)$. Using as input data the δw^2 and Ω_{Ni}^E values for a row of nodes with positions $\vec{r}_n=\vec{r}_0+x_n\vec{e}_1(x_n=n\Delta L_x)$ and 30 time values $t_k=t_0+k\Delta t(t_0=0.3\ \mu s, \Delta t=0.005\ \mu s)$, we calculated contour plots of constant δw^2 and Ω_{Ni}^E values in the (x,t) plane, with x and

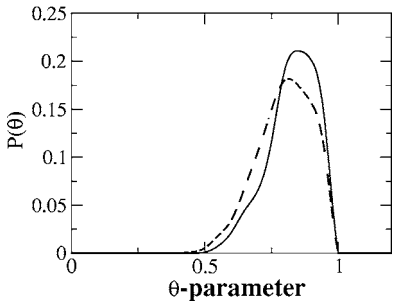

FIG. 7. Probability of the Θ_{Ni} parameter in simulated $Ni_{0.5}Zr_{0.5}$ at 700 K. Dashed line: total Ni atoms. Solid line: mobile Ni atoms.

t from interpolation of the x_n and t_k sets. The results are shown in Fig. 9 for the row of nodes from simulation box edge B to edge D of Fig. 5(a).

Clearly visible in Fig. 9 is an event of increased mobility around $x=3.5$ nm for $0.36\ \mu s<t<0.43\ \mu s$, which after a short break continues to later times. Regarding the fact that $\delta w^2(\vec{r},t,t+\Delta t_2)$ presents the accumulated effects between time t and $t+\Delta t_2$ with $\Delta t_2=0.07\ \mu s$, the observed behavior indicates a mobility event which starts around $t=0.43\ \mu s$ and which is accompanied by further dynamics at later times. A similar behavior is seen for the Ni cage volume $\Omega_{Ni}^E(\vec{r},t,t+\Delta t_2)$.

The raise in both quantities starts around $t=0.355\ \mu s$. This finding means that neither δw^2 nor Ω_{Ni}^E can be identified as the precursor of the other on the ns scale. On the other hand, the observed dynamical event takes place in a space region of enhanced Ω_{Ni}^E value, which also is characterized by slightly enhanced atomic mobility δw^2. There is a second space region of enhanced Ω_{Ni}^E value around $x=1.2$ nm, which also is characterized by a slightly enhanced δw^2 value.

The observations confirm the behavior already visible in the correlation parameters of Table II: (i) there is a correlation between δw^2 and Ω_{Ni}^E distributions at equal times. (ii) Cross correlations between the δw^2 distribution in different time regions decay strongly. (iii) Cross correlation between the Ω_{Ni}^E distribution at different time intervals decay slowly and weakly. The latter means that there is a long-living component in the Ω_{Ni}^E distribution. Regions of increased Ω_{Ni}^E values may become regions of enhanced heterogeneous mobility where, however, the enhanced mobility is accompanied by a further strong increase in the Ω_{Ni}^E value.

IV. DISCUSSION

The results described in the preceding section concern heterogeneous dynamics in the simulated vitrifying metallic $Ni_{0.5}Zr_{0.5}$ glass at $T=810$, 760, and 700 K, which means around its Kauzmann temperature $T_K\approx 750$ K [15]. The temperatures are markedly below the critical temperature T_C of the mode coupling theory ($T_C\approx 1120$ K for the present model [12,13]). This implies that there is a splitting of three orders of magnitude between the time scales of the irreversible structural dynamics and reversible thermal fluctuations [16] which allows the elimination of the reversible fluctuations by low-pass filtering of the dynamics.

TABLE I. Correlation values in simulated $Ni_{0.5}Zr_{0.5}$ at 700 K in two restricted time intervals: I_1: $t \in [0.3, 0.45\ \mu s]$ and I_2: $t \in [0.45, 0.6\ \mu s]$ and total simulation time I_0: $t \in [0, 1\ \mu s]$.

		$R(X,Y)$		
X	Y	I_1	I_2	I_0
δw^2	Ω^V_{Ni}	0.59	0.61	0.75
δw^2	Θ_{Ni}	0.66	0.64	0.77
Ω^V_{Ni}	Θ_{Ni}	0.88	0.84	0.99
δw^2	ρ_{par}	−0.03	−0.08	−0.04
δw^2	ρ_{Ni}	−0.05	−0.11	−0.1

Cross correlations		$R(X,Y)$
$\Theta(I_1)$	$\Theta(I_2)$	0.50
$\delta w^2(I_1)$	$\delta w^2(I_2)$	0.15

The main part of our analysis concentrates on the irreversible and low-frequency dynamics. By purpose we have eliminated from the dynamics all reversible vibrational fluctuations on the GHz scale and above, which by their large density tend to spoil the irreversible relaxation dynamics. The latter dynamics takes place by the formation of local clusters of mobile particles, as analyzed in detail in our recent study of a 648-atom system at 700 K [16]. The agreement of the present observations in a 5184-atom system with the earlier ones for the small system gives support to the assumptions that the local dynamical events in [16] are not induced by the smallness of the system there. On the other hand, the agreement supports the conclusion that the local dynamical events seen in the present analysis, which in essence have diameters markedly smaller than the extension of the simulation box, do not mean a finite-size effect of the present system.

TABLE II. Correlation values in simulated $Ni_{0.5}Zr_{0.5}$ at 700, 760, and 810 K in two restricted time intervals J_1: $t \in [0.2, 0.3\ \mu s]$ and J_2: $t \in [0.4, 0.5\ \mu s]$ and total simulation time J_0: $t \in [0, 0.6\ \mu s]$.

		$R(X,Y)$		
X	Y	700 K	760 K	810 K
$\delta w^2(J_0)$	$\Omega^V_{Ni}(J_0)$	0.75	0.81	0.82
$\delta w^2(J_0)$	$\Theta_{Ni}(J_0)$	0.77	0.84	0.83
$\Theta_{Ni}(J_0)$	$\Omega^V_{Ni}(J_0)$	0.99	0.96	0.99
$\delta w^2(J_0)$	$\rho_{Ni}(J_0)$	−0.10	−0.12	−0.23
$\delta w^2(J_0)$	$\rho_{par}(J_0)$	−0.07	−0.09	−0.26
$\delta w^2(J_0)$	E_{pot}	0.05	0.21	0.33
$\delta w^2(J_1)$	$\Omega^V_{Ni}(J_1)$	0.63	0.70	0.76
$\delta w^2(J_1)$	$\Theta(J_1)$	0.65	0.73	0.77
$\Theta(J_1)$	$\Omega^V_{Ni}(J_1)$	0.98	0.99	0.99
$\delta w^2(J_2)$	$\Omega^V_{Ni}(J_2)$	0.57	0.52	0.78
$\delta w^2(J_2)$	$\Theta(J_2)$	0.59	0.59	0.81
$\Theta(J_2)$	$\Omega^V_{Ni}(J_2)$	0.98	0.98	0.99
$\delta w^2(J_1)$	$\delta w^2(J_2)$	0.33	0.27	0.55
$\Omega^V_{Ni}(J_1)$	$\Omega^V_{Ni}(J_2)$	0.63	0.52	0.70
$\Theta(J_1)$	$\Theta(J_2)$	0.63	0.54	0.73
$\delta w^2(J_1)$	$\Omega^V_{Ni}(J_2)$	0.33	0.25	0.56
$\delta w^2(J_1)$	$\Theta(J_2)$	0.34	0.28	0.58
$\Theta(J_1)$	$\Omega^V_{Ni}(J_2)$	0.61	0.51	0.72
$\delta w^2(J_2)$	$\Omega^V_{Ni}(J_1)$	0.15	0.23	0.48
$\delta w^2(J_2)$	$\Theta(J_1)$	0.17	0.25	0.50
$\Theta(J_2)$	$\Omega^V_{Ni}(J_1)$	0.61	0.52	0.71

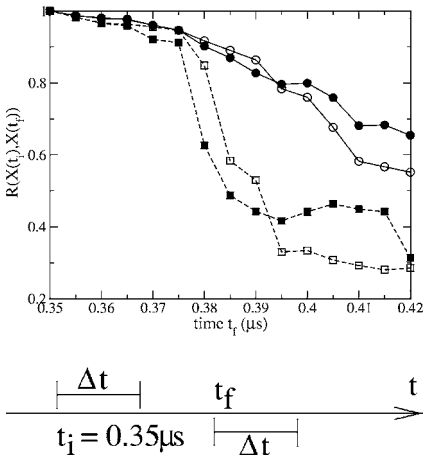

FIG. 8. (a) Correlation coefficients. X stands for cage volume around Ni atoms Ω^E_{Ni} or atomic mobility δw^2. Dashed line with solid squares: atomic mobility with time width $\Delta t = 0.1\ \mu s$. Dashed line with opened squares: atomic mobility with time width $\Delta t = 0.07\ \mu s$. Solid line with solid circles: cage volume around Ni atoms with time width $\Delta t = 0.1\ \mu s$. Solid line with open circles: cage volume around Ni atoms with time width 0.1 μs. (b) Illustration of using varying t_f and fixed t_i and constant time width when evaluating the R parameter in (a).

It is a particular feature of the present analysis that local dynamics and local structure fluctuations are ascribed by coarse graining to volume elements of the sample rather than to individual atoms. The treatment makes use of a suitable characterization of the local, heterogeneous low-frequency dynamics. The details of the structure are characterized by a number of quantities, such as local particle density and local density of Ni atoms, the spatial density of cage-size volume around Ni atoms, or the local symmetry around Ni atoms, the latter being measured by the Q_4 and Q_6 parameters and the Θ_{Ni} parameter derived there from.

The analysis displays marked correlations between the spatial distribution of the coarse-graining low-frequency mobility on the one hand and cage-size value around Ni atoms, Ω_{Ni}, and Θ_{Ni}-parameter distribution, respectively, on the other hand. In addition, we find strong correlations between the spatial distribution of cage-size values Ω_{Ni} and Θ_{Ni} parameter, which substantiates the assumption that both quantities reflect the same feature of the atomic arrangement.

The present results are in accordance with the concept of "propensity," forwarded in [10], according to which the tendency for an increased local mobility in the system already is encapsulated in the existing atomic arrangement. According to our findings, there is a long-living component in the spatial Ω_{Ni} distribution. Regions of enhanced Ω_{Ni} value seem to

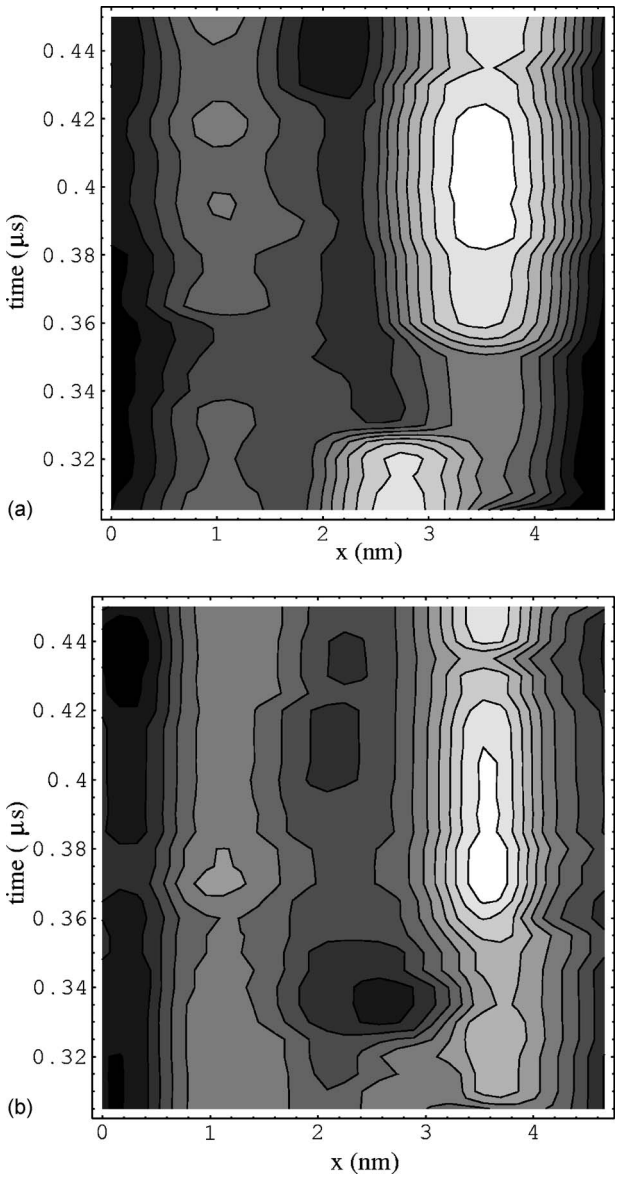

FIG. 9. (a) Space and time evolution of heterogeneous dynamics; contour values range is [0.04,10.5] (ten contours with constant distance on a log scale). (b) Space and time evolution of atomic volume contour values range is [0.84,1.26] (ten contours with constant distance on a log scale). The contour values are all normalized to the spatial average of the quantity.

be regions of the preferential initiation of irreversible low-frequency dynamics, where the enhanced mobility is accompanied by a further strong increase in the Ω_{Ni} value. For the present system we thus can specify the propensity relationship by offering the cage volume around Ni atoms as a measure of this tendency.

Regarding spatial fluctuations of the particle density, Ni-atom density, and mean potential energy per atom, there are indications for a weak anticorrelation of the former two quantities with the spatial distribution of low-frequency heterogeneous dynamics at 810 K and for a weak correlation in case of the latter. The correlations decrease with decreasing temperature and are negligibly small at 700 K. The observations for the low-frequency dynamics at 810 K are in agreement with the findings of Weeks and Weitz [3] according to which in the case of high-frequency dynamics there is a tendency for increased atomic mobility in regions of lower density. A similar agreement exists with the observations by Donati *et al.* [5] according to which the mobility of atoms increases with increasing potential energy. Moreover, taking as given that atoms with coordination number below average will have a reduced gain in potential energy, the present observation for a correlation between mean potential energy and mobility is in accordance with the results of Vollmayr-Lee, Kob, and Zippelius [7], who found a tendency of mobile atoms to be caged by fewer neighbors. Here we shall emphasize once again that our treatment differs from Refs. [3,5,7] not only regarding the considered temperature range, but basically due to the concentration on irreversible and low-frequency relaxation dynamics. On a short time scale the latter are masked by the overwhelming density of reversible thermal fluctuations, which here are eliminated by low-pass filtering. This makes it prohibitive, in particular, to relate our observations to those of Ref. [8] which clearly concerns vibrational excitations.

As we already addressed in a recent paper [16], it is tempting to correlate the here seen local dynamical events, which we identified in [16] as avalanches or cascades of collectively moving atoms, with the objects of "defect models" that currently gain increasing interest [28–30] as tools to approach the thermodynamics of the glass transition. There is, in particular, a close similarity to the idea of "dynamical facilitation" promoted by Garrahan and Chandler [28,31]. These authors consider in a coarse-grained picture volume elements in a "mobile" state, on the one hand, which carry the irreversible structural dynamics and which are rare excitations, and elements in an "immobile" state of the glass, on the other hand, which are said to provide the overwhelming contribution of reversible, thermal fluctuations [31]. Such a picture is in full agreement with our findings. One has to remember, however, that according to our so far analyzed cases [16,19] for $Ni_{0.5}Zr_{0.5}$ irreversible dynamics is due to a mutual triggering and stabilization of chains of collectively moving atoms. In the well-relaxed system at low temperatures, the chains alone, in particular those with low activation energy, turned out to be reversible excitations of the structure. According to that, the "mobile" state of a volume element seems to be closely related to the thermally activated "immobile" state of the system. There is, nevertheless, a structural difference between "mobile" and "immobile" states as is manifested by the difference in the cage volume around the Ni atoms or in the Θ_{Ni} parameter. Accordingly, there is space that "mobile" and "immobile" regions may differ in entropy, as used as an essential point in the approach by Matyushov and Angell [30].

V. CONCLUSIONS

The present investigation is concerned with the question of spatial correlations between the irreversible structural dynamics and structural inhomogeneities in a thermodynamically homogeneous amorphous system around its Kauzmann temperature, which means the range of the common experi-

mental glass temperature. An answer to this question demands the separation of irreversible and low-frequency dynamics, well below the GHz regime, from reversible high-frequency dynamics, taking place around the THz range. Our approach provides a suitable tool to achieve this separation in MD simulations, like the ones given here for binary $Ni_{0.5}Zr_{0.5}$.

For the low-frequency relaxation dynamics, the present results demonstrate the existence of non-negligible correlations in space and time between heterogeneous structural dynamics and some involved structure parameters such as our so-called Θ_{Ni} parameter, based on Steinhardt's Q_4 and Q_6 parameters or the cage volume Ω_{Ni} around Ni atoms, measured by either Egami's approach or a Voronoi construction. Since the cross-correlation values among the fluctuations of these structural parameters turn out in the range of 0.9, there is strong support that they reflect one and the same physical property.

Cross-correlation values of these parameters with the heterogeneous low-frequency dynamics are of the order of 0.6, which indicates that there exist correlations between the spatial distributions of these quantities. There are long-living regions of enhanced Ω_{Ni} values in the system. Our results give some support to the assumption that these regions are the regions of preferential initiation of irreversible low-frequency dynamics where, however, activation of a local, irreversible dynamical event increases temporarily the local Ω_{Ni} value further.

Cross correlations between irreversible low-frequency dynamics and structure parameters like total particle density, Ni-atom density, or mean potential energy of the atoms turned out to be small with absolute values of the correlation parameter R between 0.33, and 0.23 at 810 K and absolute values of R below 0.21 at 700 and 760 K, respectively. Thus, for the present temperature range and the present system, these parameters seem not well suited to distinguish regions of heterogeneous, irreversible dynamics from immobile regions on the low-frequency scale. Regarding the observed increase of $|R|$ with temperature, our data substantiate, however, the assumption that at 810 K and above there may exist weak anticorrelations between mobility and total particle and Ni-atom density, respectively, as well as a weak correlation with mean potential energy per atom.

ACKNOWLEDGMENT

The authors gratefully acknowledge support through the ZAM Jülich by providing computer capacity on the JUMP system for carrying out the calculations.

[1] G. Adam and J. H. Gibbs, J. Chem. Phys. **43**, 139 (1965).
[2] M. D. Ediger, Annu. Rev. Phys. Chem. **51**, 99 (2000).
[3] E. R. Weeks and D. A. Weitz, Phys. Rev. Lett. **89**, 095704 (2002).
[4] A. K. Sood, in *Solid State Physics*, edited by H. Ehrenreich and D. Turnbull (Academic Press, New York), 1991), Vol. 45, pp. 1–73.
[5] C. Donati, S. C. Glotzer, P. H. Poole, W. Kob, and S. J. Plimpton, Phys. Rev. E **60**, 3107 (1999).
[6] D. N. Perera and P. Harrowell, J. Chem. Phys. **111**, 5441 (1999).
[7] K. Vollmayr-Lee, W. Kob, and A. Zippelius, J. Chem. Phys. **116**, 5158 (2002).
[8] V. A. Luchnikov, N. N. Medvedev, Yu. I. Naberukhin, and V. N. Novikov, Phys. Rev. B **51**, 15569 (1995).
[9] S. Büchner and A. Heuer, Phys. Rev. Lett. **84**, 2168 (2000).
[10] A. Widmer-Cooper, P. Harrowell, and H. Fynewever, Phys. Rev. Lett. **93**, 135701 (2004).
[11] W. Götze and L. Sjögren, Rep. Prog. Phys. **55**, 241 (1992).
[12] H. Teichler, Phys. Rev. Lett. **76**, 62 (1996).
[13] H. Teichler, Phys. Rev. E **53**, R4287 (1996).
[14] W. Kauzmann, Chem. Rev. (Washington, D.C.) **43**, 219 (1948).
[15] H. Teichler, Phys. Rev. B **59**, 8473 (1999).
[16] H. Teichler, Phys. Rev. E **71**, 031505 (2005).
[17] C. Hausleitner and J. Hafner, Phys. Rev. B **45**, 115 (1992).
[18] K. Brinkmann and H. Teichler, Phys. Rev. B **66**, 184205 (2002).
[19] H. Teichler, J. Non-Cryst. Solids **293-295**, 339 (2001).
[20] B. Böddeker and H. Teichler, Phys. Rev. E **59**, 1948 (1999).
[21] F. P. Preparata and M. I. Shamos, *Computational Geometry: An Introduction* (Springer-Verlag, New York, 1985).
[22] T. Egami, K. Maeda, and V. Vitek, Philos. Mag. A **41**, 883 (1980).
[23] D. Srolovitz, K. Maeda, and T. Egami, Philos. Mag. A **44**, 847 (1981).
[24] P. J. Steinhardt, D. R. Nelson, and M. Ronchetti, Phys. Rev. B **28**, 784 (1983).
[25] J. P. Hansen and I. R. McDonald, *Theory of Simple Liquids* (Academic, New York, 1976).
[26] R. S. Averback, Mater. Res. Bull. **16**, 47 (1991).
[27] Y. Gebremichael, T. B. Schrøder, F. W. Starr, and S. C. Glotzer, Phys. Rev. E **64**, 051503 (2001).
[28] D. Chandler and J. D. Garrahan, J. Chem. Phys. **123**, 044511 (2005).
[29] G. Biroli, J. P. Bouchaud, and G. Tarjus, J. Chem. Phys. **123**, 044510 (2005).
[30] D. V. Matyushov and C. A. Angell, J. Chem. Phys. **123**, 034506 (2005).
[31] J. P. Garrahan and D. Chandler, Phys. Rev. Lett. **89**, 035704 (2002).